

# Graphene-based Plasmonic Nano-Antenna for Terahertz Band Communication in Nanonetworks

Josep Miquel Jornet, *Member, IEEE*, and Ian F. Akyildiz, *Fellow, IEEE*

**Abstract**—Nanonetworks, i.e., networks of nano-sized devices, are the enabling technology of long-awaited applications in the biological, industrial and military fields. For the time being, the size and power constraints of nano-devices limit the applicability of classical wireless communication in nanonetworks. Alternatively, nanomaterials can be used to enable electromagnetic (EM) communication among nano-devices. In this paper, a novel graphene-based nano-antenna, which exploits the behavior of Surface Plasmon Polariton (SPP) waves in semi-finite size Graphene Nanoribbons (GNRs), is proposed, modeled and analyzed. First, the conductivity of GNRs is analytically and numerically studied by starting from the Kubo formalism to capture the impact of the electron lateral confinement in GNRs. Second, the propagation of SPP waves in GNRs is analytically and numerically investigated, and the SPP wave vector and propagation length are computed. Finally, the nano-antenna is modeled as a resonant plasmonic cavity, and its frequency response is determined. The results show that, by exploiting the high mode compression factor of SPP waves in GNRs, graphene-based plasmonic nano-antennas are able to operate at much lower frequencies than their metallic counterparts, e.g., the Terahertz Band for a one-micrometer-long ten-nanometers-wide antenna. This result has the potential to enable EM communication in nanonetworks.

**Index Terms**—Nano-antenna, graphene, plasmonics, terahertz band, nanonetworks.

## I. INTRODUCTION

NANOTECHNOLOGY is providing a new set of tools to the engineering community to design and manufacture novel electronic components, a few cubic nanometers in size, which can perform specific functions, such as computing, data storing, sensing and actuation. The integration of several nano-components into a single entity, just a few cubic micrometers in size, will enable the development of more advanced nano-devices. By means of communication, these nano-devices will be able to achieve complex tasks in a distributed manner [1]. The resulting *nanonetworks will enable unique applications* of nanotechnology in the biomedical, industrial, environmental and military fields, such as advanced health monitoring and drug delivery systems, or wireless nanosensor networks for biological and chemical attack prevention.

For the time being, *enabling the communication among nano-devices* is still an unsolved challenge. The miniaturization of a classical antenna to meet the size requirements of nano-devices would impose very high radiation frequencies.

Manuscript received July 31, 2012; revised November 3, 2012.

J. M. Jornet is with the Department of Electrical Engineering, University at Buffalo, The State University of New York, Buffalo, NY, 14260, USA (e-mail: jmjornet@buffalo.edu).

I. F. Akyildiz is with the School of Electrical and Computer Engineering, Georgia Institute of Technology, Atlanta, GA, 30332, USA (e-mail: ian@ece.gatech.edu).

Digital Object Identifier 10.1109/JSAC.2013.SUP2.1213001

For example, a one-micrometer-long dipole antenna would resonate at approximately 150 THz. The available transmission bandwidth increases with the antenna resonant frequency, but so does the propagation loss. Due to the expectedly very limited power of nano-devices [40], the feasibility of nanonetworks would be compromised if this approach were followed. In addition, it is not clear how a miniature transceiver could be engineered to operate at these very high frequencies. Moreover, intrinsic material properties of common metals remain unknown at the nanoscale [4], [13] and, thus, common assumptions in antenna theory, such as the ideal Perfect Electric Conductor (PEC) behavior of the antenna building components, do not hold in this realm.

Alternatively, the use of *nanomaterials to fabricate miniature antennas* can help to overcome these limitations [3], [4], [13], [18], [22], [25], [32]. Amongst others, graphene, i.e., a one-atom thick layer of carbon atoms in a honeycomb crystal lattice [10], [27], has attracted the attention of the scientific community due to its unique electronic and optical properties. Amongst others, the conductivity of graphene has been studied both for DC and for frequencies that range from the Terahertz Band (0.1-10 THz) up to the visible spectrum [8], [9], [11], [12], [28], [35]. In particular, it has been shown that it drastically changes with the dimensions or the chemical potential. For example, the infrared conductivity of *infinitely large two-dimensional graphene sheets* at zero chemical potential has been found to be essentially independent of frequency and equal to  $\sigma_0 = \pi e^2/2h$  (where  $e$  refers to the electron charge and  $h$  refers to the Planck constant). More interestingly, it has been recently shown that the lateral confinement of electrons in *semi-finite-size graphene nanoribbons (GNRs)* enhances the material conductivity in the Terahertz Band [15], [29].

In accordance to its conductivity, the propagation of *Surface Plasmon Polariton (SPP) waves* on doped graphene has been recently analytically studied and experimentally proved [6], [16], [19], [20], [24], [26], [33], [37]. SPP waves are confined EM waves coupled to the surface electric charges at the interface between a metal and a dielectric material. Many metals support the propagation of SPP waves, but usually at very high frequencies (e.g., near-infrared and optical frequency bands). In addition, the propagation of SPP waves even on noble metals, which are considered the best plasmonic materials [41], exhibit large Ohmic losses and cannot be easily tuned. On the contrary, SPP waves on graphene have been observed at frequencies as low as in the Terahertz Band and, in addition, these can be tuned by means of material doping.

The propagation wave vector of SPP waves in graphene can be up to two orders of magnitude above the propagation

wave vector in vacuum. This can be exploited to design *plasmonic nano-antennas*, as we firstly proposed in [18]. The main difference between a metallic antenna and a plasmonic antenna is that the equivalent electrical size of a plasmonic antenna is much larger than its physical dimensions, due to the much lower speed of SPP waves in the plasmonic antenna compared to that of free-space EM waves in classical antennas. This results in much more compact antennas which can be integrated into nano-devices. Plasmonic antennas are not a new concept, but have been investigated before [5], [7], [21], [23]. The main difference between classical plasmonic antennas and graphene-based plasmonic antennas is that SPP waves in graphene are observed at frequencies in the Terahertz Band, i.e., two orders of magnitude below SPP waves observed in gold and other noble materials. In addition, graphene SPP waves can be tuned by material doping, which opens the door to tunable nano-antennas. However, to the best of our knowledge, an accurate analysis of the impact of the lateral confinement of electrons in GNRs and chemical potential on, first, the propagation of SPP waves in GNRs and, second, on the plasmonic nano-antenna response, is missing.

In this paper, we propose, model and analyze a *graphene-based plasmonic nano-antenna* for Terahertz Band communication in nanonetworks, which reassembles a *nano-strip antenna* (see Fig. 1). A mathematical framework is developed to analyze the impact of the dimensions and chemical potential on the conductivity of the GNR, the propagation properties of the SPP waves in GNRs, and the frequency response of the plasmonic nano-antenna. The results show that by exploiting the behavior of SPP waves in GNRs, miniature graphene-based plasmonic nano-antennas are able to operate at much lower frequencies than their metallic counterparts. For example, a one-micrometer-long few nanometers-wide nano-antenna is expected to radiate in the Terahertz Band. This makes graphene-based nano-antennas a promising enabling technology for EM communication in nanonetworks.

The contributions of this paper are summarized as follows:

- We analytically and numerically study the dynamic complex conductivity of GNRs by using the Kubo formalism, and investigate the impact of the electron lateral confinement and chemical potential on the GNR EM response.
- We analytically derive the dynamic complex wave vector of SPP waves in GNRs, and numerically determine the mode compression factor and the propagation length of SPP waves in GNRs, for the first time.
- We model the proposed graphene-based heterostructure as a plasmonic resonant cavity and analytically obtain its frequency response for different parameter values.

The remainder of this paper is organized as follows. In Section II, we describe the working principle of our proposed nano-antenna. In Section III, we analytically and numerically investigate the conductivity of GNRs. In Section IV, we analytically and numerically investigate the propagation and compute the dynamic complex wave vector of SPP waves in GNRs. In Section V, we obtain the nano-antenna frequency response, and we conclude the paper in Section VI.

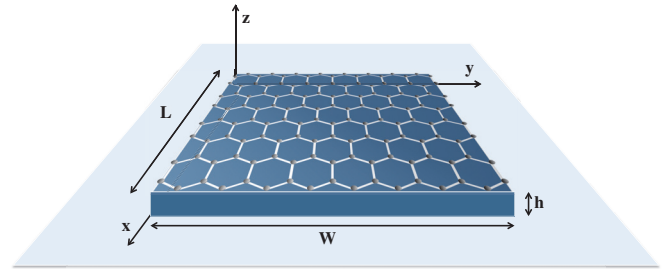


Fig. 1. A graphene-based plasmonic nano-patch antenna.

## II. GRAPHENE-BASED PLASMONIC NANO-ANTENNA

The conceptual design of the proposed graphene-based plasmonic nano-antenna is shown in Fig. 1. The nano-antenna is composed of a GNR (the active element), mounted over a metallic flat surface (the ground plane), with a dielectric material layer in between, which is used both to support the GNR as well as to change its chemical potential by means of material doping. In the complete model, an ohmic contact or a mechanism to feed the antenna is necessary. However, the design of adequate feeding mechanisms for nano-antennas is not the scope of this paper, but part of our future work.

The working principle of the nano-antenna is as follows. For simplicity, we explain first the device functioning in reception:

- Consider an incident EM plane wave,  $\vec{E}_{inc}$ , given by

$$\vec{E}_{inc}(z, t) = E_0 e^{i(-k_1 z + \omega t)} \hat{\alpha}, \quad (1)$$

where  $E_0$  is the field amplitude,  $k_1$  is the propagation constant in medium 1 (above the GNR),  $-z$  is the propagation direction (perpendicular to the GNR, see Fig. 1),  $\omega$  is the angular frequency,  $t$  stands for time and  $\alpha = x, y$  is the wave polarization. When  $\vec{E}_{inc}$  irradiates the antenna, it excites the free electrons on the graphene layer. The electronic response of the graphene layer to an EM field is given by its dynamic complex conductivity,  $\sigma$ . The conductivity of the GNR depends on the GNR edge geometry, width and chemical potential, and the incident field polarization  $\alpha$ . In Section III, we study in detail the dynamic complex conductivity  $\sigma$  of GNRs.

- At the interface between the graphene layer and the dielectric material layer, SPP waves are excited. The SPP wave modes that can be supported on the GNR and their dynamic complex wave vector  $k_{spp}$  depend on the real and imaginary part of the dynamic complex conductivity,  $\sigma$ . In Section IV, we study the propagation of Transverse Magnetic and Electric SPP modes in GNRs and obtain an analytical expression for their dynamic complex wave vector,  $k_{spp}$ . Extensive numerical results are provided to understand the properties of SPP modes, e.g., the SPP mode compression factor and the propagation length, which are analyzed in GNRs for the first time.
- By exploiting the high mode compression factor of SPP waves in GNRs, novel graphene-based plasmonic nano-antennas can be developed. The main difference between conventional PEC antennas and plasmonic antennas is the fact that the SPP current wave propagates with a much larger wave vector than conventional electric current waves in PEC antennas. This results in a much lower

resonant frequency of plasmonic antennas. The frequency response of nano-antennas is described and analyzed in Section V, by modeling the antenna as a resonant cavity.

According to the *antenna reciprocity theorem*, the behavior of the nano-antenna in transmission can similarly be explained as follows. Consider a time-varying electric current,  $\vec{J}$ ,

$$\vec{J}(z, t) = J_0 e^{i\omega t} \delta(z - h) \hat{\alpha} \quad (2)$$

where  $J_0$  is the current amplitude,  $\omega$  is the angular frequency,  $t$  stands for time,  $\delta$  stands for the Dirac delta function,  $h$  is the  $z$  coordinate of the GNR, i.e., the separation between the ground plane and the GNR itself, and corresponds to the feeding point (see Fig. 1), and  $\alpha = x, y$  is the current direction. When  $\vec{J}$  excites the graphene layer, an SPP wave is generated at the interface with the dielectric material layer. If the length of the graphene patch corresponds to integer number of half plasmon wavelengths,  $\lambda_{spp}$ , the plasmonic antenna resonates, and the antenna radiated EM field is maximized, as we show in Section V. Ultimately, the frequency response and efficiency of nano-antennas depends on the properties of SPP waves, which on their turn depend on the conductivity of GNRs.

### III. CONDUCTIVITY OF GRAPHENE NANORIBBONS

In this section, we analytically and numerically investigate the conductivity of GNRs. For this, first, we recall the electronic band structure and the electron wave functions of GNRs, and, then, we use the Kubo formalism to study the conductivity of GNRs as a function of their width and chemical potential.

#### A. Electronic Band Structure and Electron Wave Functions

The electronic band structure of a GNR, which describes the energy values that an electron is allowed or forbidden to have, depends on the geometry across its long edge. In this paper, we focus on Armchair GNRs (AGNRs) (see Fig. 2 (left)), but a similar study can be conducted for Zigzag GNRs (ZGNRs), with or without defects [29]. The electronic band structure  $\varepsilon$  in electron-volts (eV) of an AGNR is given by [38]

$$\varepsilon^s(k, \theta) = st \sqrt{1 + 4 \cos^2 \theta + 4 \cos \theta \cos\left(\frac{kb}{2}\right)}, \quad (3)$$

where  $s$  is the band index ( $s = 1$  for the conduction band,  $s = -1$  for the valence band),  $t \approx 3$  eV is the nearest-neighbor atom interaction in the tight-binding model of graphene,  $k$  and  $\theta$  are the wave vectors parallel and perpendicular to the AGNR edge, respectively, and  $b = 3a_0$ , where  $a_0 = 0.142$  nm is the graphene lattice constant. The Brillouin zone, i.e., the area of interest in the wave vector domain, is the region defined by the values of  $kb \in [0, \pi)$  and  $\theta \in (0, \pi)$ . The conduction and the valence bands touch at the point  $(k, \theta) = (0, 2\pi/3)$ , which is referred to as the Dirac point.

Due to the finite width  $W$  of the AGNR, the values of  $\theta$  are quantized. In particular, by defining the AGNR width as  $W = \sqrt{3}/2 a_0 (N - 1)$ , with  $N$  being the number of single-atom columns across the AGNR width (see Fig. 2 (left)), the values of  $\theta$  are given by

$$\theta_n = \frac{n\pi}{N + 1}, \quad (4)$$

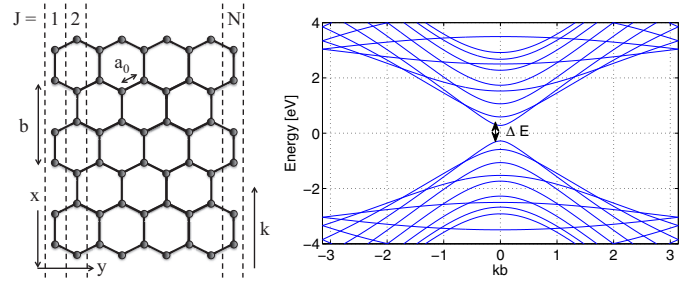


Fig. 2. Lattice structure of an AGNR (left) and energy band-structure an AGNR with  $N = 18$  ( $\Delta E = 0.56$  eV).

where  $n = 1, 2, \dots, N$  stands for the band index. By considering the GNR length  $L$  much larger than its width, the wave vector  $k$  is treated as a continuous variable. In our analysis,  $L$  is in the order of several hundreds of nanometers and up to one micrometer, and  $L \gg W$ .

The wave functions  $\Phi_J^s$  in an AGNR are given by [31]

$$\phi_J^s(k, \theta_n) = \frac{1}{\sqrt{N}} e^{-ik \frac{b}{2} (J-1)} \sin J \theta_n \begin{pmatrix} e^{-i\Theta(k, \theta_n)} \\ s \end{pmatrix}, \quad (5)$$

where  $J = 1, 2, \dots, N$  is the single-atom column index across the AGNR width (see Fig. 2 a)) and  $\Theta$  is the polar angle between  $k$  and  $\theta_n$  defined with respect to the Dirac point and it is given by

$$\Theta(k, \theta_n) = \text{atan}\left(\frac{kb}{\theta_n - \frac{2\pi}{3}}\right), \quad (6)$$

where  $\text{atan}$  refers to the inverse trigonometric tangent function and  $\theta_n$  is defined as in (4).

In Fig. 2 (right), the energy band structure  $\varepsilon$  of an AGNR, given by (3), with width  $W \approx 2.1$  nm ( $N = 18$ ) is shown. For this width, the AGNR has a semi-conducting behavior, i.e., there is a gap between the valence and the conduction bands. The energy bandgap  $\Delta E$  in AGNRs depends on  $N$  and is given in eV by

$$\Delta E = \begin{cases} 0, & N = 3m - 1, \\ -2t \left[ 1 + \cos\left(\frac{2m+1}{3m+1}\pi\right) \right], & N = 3m, \\ -2t \left[ 1 + \cos\left(\frac{2m+1}{3m+2}\pi\right) \right], & N = 3m + 1, \end{cases} \quad (7)$$

where  $m = 1, 2, \dots$ . As we show next, the energy bandgap  $\Delta E$  plays a major role in the conductivity of thin AGNRs. In the rest of this paper, we use the following nomenclature for simplicity:  $\varepsilon_n^s = \varepsilon^s(k, \theta_n)$ ,  $\Theta^n = \Theta(k, \theta_n)$ .

#### B. Dynamical Complex Conductivity

The dynamical complex conductivity of AGNRs is computed next by means of the Kubo formalism. Following the procedure described in [15], [29], and contrary to many existing conductivity analysis which are only valid for infinitely large graphene sheets [8], [9], [11], [12], [28], [35], we do not make any simplifying assumption on the energy band structure of AGNRs, temperature or chemical potential. Simply stated, we compute the conductivity by counting all the allowed electron transitions in the energy band structure.

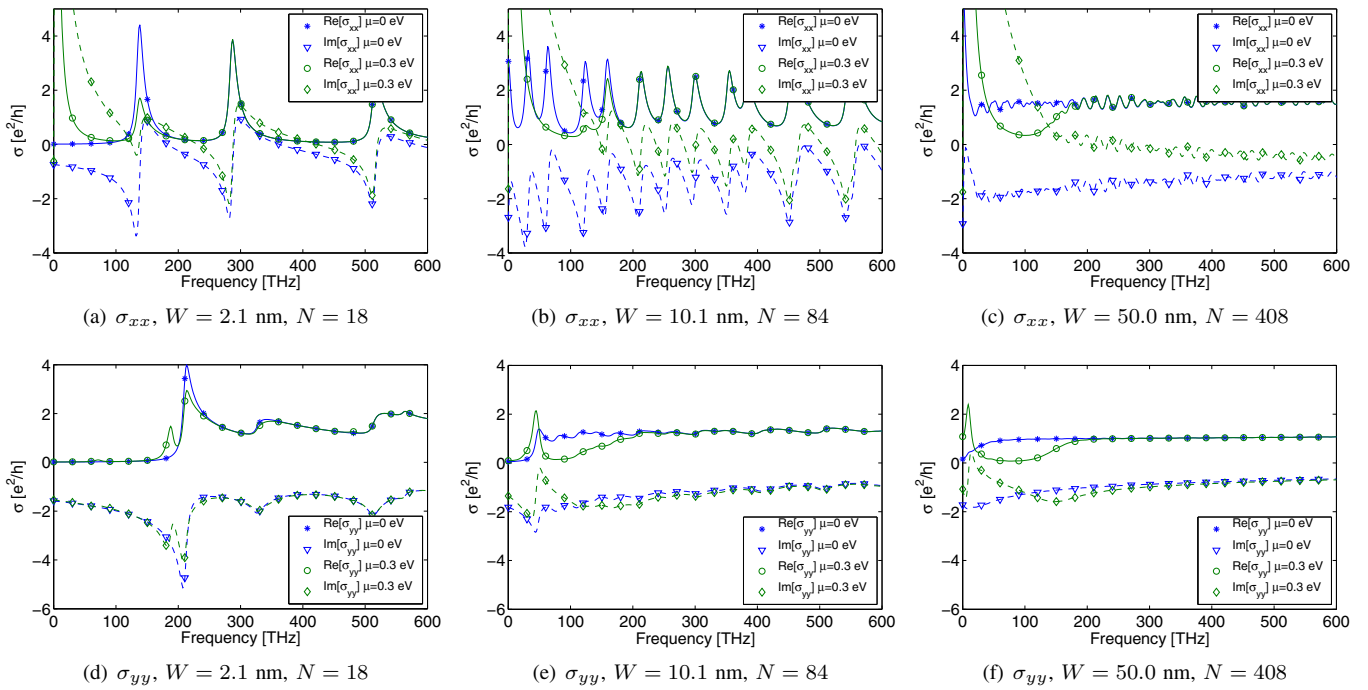


Fig. 3. Conductivity of AGNRs.

The dynamical complex conductivity  $\sigma$  of AGNRs depends on the polarization of the incident electromagnetic field ( $\alpha = x, y$ ), and it is given by

$$\sigma_{\alpha\alpha}(f) = i \frac{\hbar e^2}{S} \sum_{s,s'} \sum_{n,m} \int_k \frac{(n_F(\varepsilon_m^{s'}) - n_F(\varepsilon_n^s))}{(\varepsilon_n^s - \varepsilon_m^{s'})} \frac{|\langle \phi_m^{s'} | v_\alpha | \phi_n^s \rangle|^2}{(\varepsilon_n^s - \varepsilon_m^{s'} + \hbar f - i\nu)} dk, \quad (8)$$

where  $f$  stands for frequency in Hz,  $\hbar$  is the reduced Planck constant in eV·s,  $e$  is the electron charge in C,  $S$  is the area of the reference unit structure [2],  $\{s, s'\}$  stand for band indexes,  $\{n, m\}$  refer to the sub-bands indexes,  $k$  is the wave vector parallel to the AGNR edge,  $n_F$  is the Fermi-Dirac distribution given by

$$n_F(\varepsilon) = \frac{1}{1 + e^{\frac{\varepsilon - \mu}{k_B T}}}, \quad (9)$$

where  $\mu$  is the chemical potential in eV,  $k_B$  is the Boltzmann constant in eV/K, and  $T$  stands for the temperature in K.  $\langle \phi_m^{s'} | v_\alpha | \phi_n^s \rangle$  is the matrix element of the  $\alpha$  component of the velocity operator for the transition from the energy state  $\{s, n\}$  to the energy state  $\{s', m\}$ . The matrix elements are classified into inter-band transitions ( $s \neq s'$ ) and intra-band transitions ( $s = s'$ ). The matrix elements of velocity operator for intra-band transitions in AGNRs are obtained in [29], [30], and are given by

$$\langle \phi_m^c | v_x | \phi_n^c \rangle = \begin{cases} 0, & m - n \in \text{even}, \\ -i \frac{2}{\pi} \frac{v_F}{m-n} \langle \zeta_x \rangle_{m,n}, & m - n \in \text{odd}, \end{cases} \quad (10)$$

$$\langle \phi_m^c | v_y | \phi_n^c \rangle = \delta_{m,n} v_F \langle \zeta_y \rangle_{m,n}, \quad (11)$$

where  $v_F = tb/(2\hbar)$  is the Fermi velocity,  $\delta_{m,n}$  refers to the Kronecker delta, and  $\langle \zeta_\alpha \rangle$  ( $\alpha = x, y$ ) stands for the Pauli

matrixes, whose elements are given by

$$\langle \zeta_x \rangle_{m,n} = \frac{1}{2} (e^{i\Theta^m} + e^{-i\Theta^n}), \quad \langle \zeta_y \rangle_{m,n} = \frac{-i}{2} (e^{i\Theta^m} - e^{-i\Theta^n}), \quad (12)$$

and the polar angle  $\Theta^n$  is defined in (6). Similarly, the matrix elements of velocity operator for inter-band transitions in AGNRs are given by

$$\langle \phi_m^c | v_x | \phi_n^v \rangle = \begin{cases} 0, & m - n \in \text{even}, \\ -\frac{2}{\pi} \frac{v_F}{m-n} \langle \zeta_y \rangle_{m,n}, & m - n \in \text{odd}, \end{cases} \quad (13)$$

$$\langle \phi_m^c | v_y | \phi_n^v \rangle = \delta_{m,n} v_F \langle \zeta_x \rangle_{m,n}. \quad (14)$$

The details to derive (10), (11), (13) and (14) are given in [29]. Finally, the parameter  $\nu$  in (8) refers to the inverse of the relaxation time. Note that in (8), when  $s = s'$  and  $m = n$ , both the numerator and the denominator vanish. However, by using the Taylor expansion of the Fermi-Dirac distribution function, we can rewrite (8) for this specific case as

$$\sigma_{\alpha\alpha}(f) \approx i \frac{\hbar e^2}{S} \sum_{s,s'} \sum_{n,m} \int_k \frac{e^{\frac{\varepsilon_m^{s'} - \mu}{k_B T}} n_F(\varepsilon_m^{s'}) n_F(\varepsilon_n^s)}{k_B T} \frac{|\langle \phi_m^{s'} | v_\alpha | \phi_n^s \rangle|^2}{(\varepsilon_n^s - \varepsilon_m^{s'} + \hbar f - i\nu)} dk. \quad (15)$$

A semi-closed-form expression for the real part of the conductivity is given [15]. However, for the characterization of the SPP waves in AGNRs, both the real part and the imaginary part of  $\sigma$  are necessary. Next, we numerically study the complex conductivity of AGNRs.

### C. Numerical Analysis

In Fig. 3, the real and imaginary parts of  $\sigma_{xx}$  and  $\sigma_{yy}$  given by (8) are plotted as functions of the frequency for three

different GNR widths  $W = 2.1$  nm ( $N = 18$ ),  $W = 10.1$  nm ( $N = 84$ ) and  $W = 50.0$  nm ( $N = 408$ ), and for two different chemical potentials  $\mu = 0$  eV and  $\mu = 0.3$  eV, at  $T = 300$  K. We use  $\nu = 20$  meV, which corresponds to a relaxation time  $\tau = \hbar/\nu = 0.2$  ps, which is a conservative value.

For  $W = 2.1$  nm,  $\mu = 0$  eV, the conductivity,  $\sigma_{xx}$ , along the AGNR edge is dominated by inter-band transitions. The first peak in the real part of  $\sigma_{xx}$  corresponds to  $f_0 = \Delta E/\hbar$ , where  $\Delta E$  is the energy band gap given by (7). When the conductivity is dominated by inter-band transitions, the imaginary part of  $\sigma_{xx}$  is negative. The sign of the imaginary part of the conductivity plays a major role in the propagation of SPP waves, as we discuss in Section IV. When the chemical potential is  $\mu = 0.3$  eV, the inter-band transitions below  $f_\mu = \mu/\hbar = 72.5$  THz disappear. This is better seen for wider GNRs. When the chemical potential is increased, a component close to 0 Hz appears due to intra-band transitions.

On its turn, the conductivity,  $\sigma_{yy}$ , across the AGNR width, is also dominated by inter-band transitions. However, there is only one peak at a frequency above the first inter-band transition frequency  $f_0$ . This peak corresponds to an indirect inter-band transition between sub-band  $n$  in the valence band and sub-band  $n - 1$  in the conduction band. Note that inter-band transitions between sub-bands with  $m = n$  are not allowed (13), as explained in [29]. When  $\mu = 0.3$  eV,  $\sigma_{yy}$  is almost unaltered. Note that there is no component close to  $f = 0$  Hz in this case, because the diagonal elements of the velocity operator  $m = n$  are equal to 0.

The behavior of the conductivity for  $W = 10.1$  nm is similar. The conductivity,  $\sigma_{xx}$  along the AGNR edge is dominated by inter-band transitions. The first peak appears at a much lower frequency, due to the fact that the energy band gap decreases with the AGNR width. When the chemical potential is increased, the inter-band transitions below  $f_\mu = \mu/\hbar = 72.5$  THz disappear. This turns into an increased conductivity component for  $f = 0$  Hz, attributed to intra-band transitions. Note that the imaginary part of the conductivity is positive when it is mainly governed by intra-band transitions.

Similarly, the conductivity  $\sigma_{yy}$  across the AGNR width is dominated by a single peak, corresponding to inter-band transitions. After that, the conductivity tends to the well-known minimum value for the optical conductivity of graphene, which further validates these numerical results. When the chemical potential is increased to  $\mu = 0.3$  eV, intra-band transitions create the peak at  $f = 0$  Hz for  $\sigma_{xx}$ . Similarly for  $\sigma_{yy}$ , forward intra-band transitions create the peak at lower frequencies. Finally, a similar behavior can be observed for  $W = 50.0$  nm. The conductivity  $\sigma_{xx}$  tends to that of infinitely large graphene sheets, and similarly occurs with  $\sigma_{yy}$ .

#### IV. SURFACE PLASMON POLARITON WAVES IN GRAPHENE NANORIBBONS

Surface Plasmon Polariton (SPP) waves are confined EM waves coupled to surface electric charges at the interface between a metal and a dielectric material. Up to now, most of the SPP-related research has been focused on the propagation of SPP waves in noble metals, such as gold and silver. These materials support the propagation of SPP waves with

high propagation lengths, in the order of a few tens of SPP wavelengths  $\lambda_{spp}$  [36]. However, noble metals only support SPP waves at frequencies in the infrared and visible frequency region (in the order of several hundreds of Terahertz). On the contrary, as we show next, graphene supports the propagation of SPP waves at much lower frequencies than the noble metals.

In this section, we analytically compute the dynamic complex wave vector of SPP waves in AGNRs and numerically study their main propagation properties. The majority of existing studies [6], [14], [17], [20] are focused on infinitely large graphene sheets. Only recently in [33], the dielectric function of GNRs is utilized to investigate SPP waves in metallic AGNRs. Next, we capture the impact of the finite width of AGNRs and the chemical potential on the SPP waves.

##### A. Dynamic Complex Wave Vector

The dynamic complex wave vector  $k_{spp}$  of SPP waves in graphene determines the propagation properties of SPP waves.  $k_{spp}$  strongly depends on the conductivity of the AGNR  $\sigma_{\alpha\alpha}$  as well as the permeability  $\mu_n$  and permittivity  $\epsilon_n$  of the materials surrounding the AGNR. The real part of the wave vector,

$$\text{Re}\{k_{spp}\} = \frac{2\pi}{\lambda_{spp}}, \quad (16)$$

determines the SPP wavelength. The imaginary part of the wave vector  $\text{Im}\{k_{spp}\}$  determines the SPP decay or, inversely,  $1/\text{Im}\{k_{spp}\}$  determines the SPP propagation length. We proceed next to compute the complex value of  $k_{spp}$ .

In reception, an  $\alpha$ -polarized incident EM plane wave (1) excites a SPP wave mode on the AGNR, which propagates in the  $\alpha$  direction. Two types of SPP modes can be supported by the AGNR depending on its conductivity:

- Transverse Magnetic (TM) mode: there is no magnetic field in the direction of propagation, i.e.,  $H_\alpha = 0$ .
- Transverse Electric (TE) mode: there is no electric field in the direction of propagation, i.e.,  $E_\alpha = 0$ .

1) **TM Modes:** In order to determine the wave vector  $k_{spp}$  for TM modes we proceed as follows. The SPP electric field  $\vec{E}$  and magnetic field  $\vec{H}$  are governed by the Maxwell's equations, which can be written in their differential form as:

$$\nabla \times \vec{E} = -\mu_n \frac{\partial \vec{H}}{\partial t}, \quad \nabla \times \vec{H} = \vec{J} + \epsilon_n \frac{\partial \vec{E}}{\partial t}, \quad (17)$$

where  $\nabla \times$  is the curl operator,  $\mu_n = \mu_0 \mu_n^r$  is the permeability of medium  $n$  ( $n = 1$  above the AGNR,  $n = 2$  below the AGNR),  $\epsilon_n = \epsilon_0 \epsilon_n^r$  is the permittivity of medium  $n$ , and  $\vec{J}$  is the current created by the  $\alpha$ -component of the electric field,  $E_\alpha$ , given by

$$\vec{J} = \sigma_{\alpha\alpha} E_\alpha \delta(z-h) \hat{\alpha}, \quad (18)$$

where  $\sigma_{\alpha\alpha}$  is the AGNR conductivity given by (8) and  $h$  is the  $z$  coordinate of the AGNR.

The complex propagation index of TM modes can be found by assuming that the electric field  $\vec{E}$  has the form:

$$\begin{aligned} \vec{E} &= E_1 e^{i(k_{spp}\alpha - k_1(z-h))} \hat{\alpha} + E_2 e^{i(k_{spp}\alpha - k_1(z-h))} \hat{z} & z \geq h, \\ \vec{E} &= E_3 e^{i(k_{spp}\alpha + k_2(z-h))} \hat{\alpha} + E_4 e^{i(k_{spp}\alpha + k_2(z-h))} \hat{z} & z < h, \end{aligned} \quad (19)$$

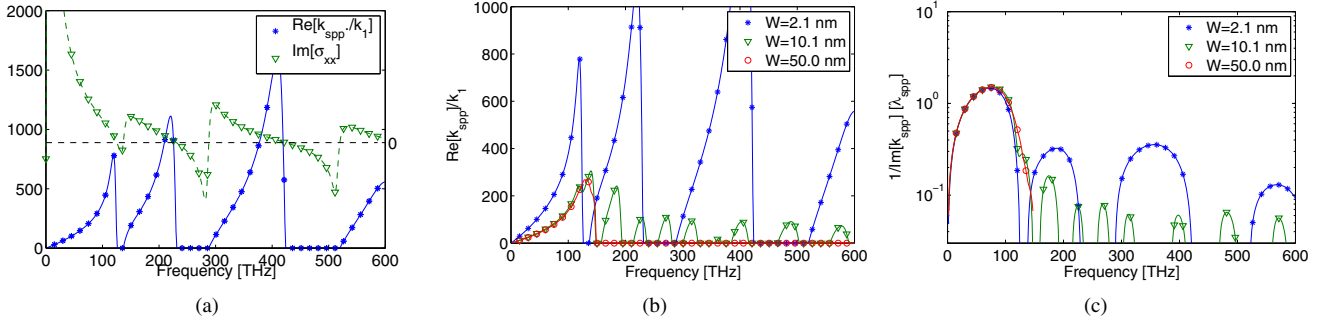


Fig. 4. (a) Real part of  $k_{spp}/k_1$  and imaginary part of  $\sigma_{xx}$  for an AGNR with  $W = 2.1$  nm, (b) Real part of  $k_{spp}/k_1$  for different AGNR width, and (c)  $1/e$ -amplitude decay propagation distance in terms of  $\lambda_{spp}$  for different AGNR width ( $\mu = 0.3$  eV,  $T = 300$  K).

and the magnetic field  $\vec{H}$  has the form:

$$\begin{aligned} \vec{H} &= H_1 e^{i(k_{spp}\alpha - k_1(z-h))} \hat{\alpha}' & z \geq h, \\ \vec{H} &= H_2 e^{i(k_{spp}\alpha + k_2(z-h))} \hat{\alpha}' & z < h, \end{aligned} \quad (20)$$

where  $E_1, E_2, E_3, E_4, H_1$  and  $H_2$  are constants,  $k_{spp}$  is the SPP wave vector,  $\hat{\alpha}$  is the polarization direction,  $\hat{\alpha}' = |\hat{\alpha} \times \hat{z}|$  and  $k_n$  is the wvector in medium  $n$  given by:

$$k_n = \frac{2\pi}{\lambda_n} = \omega \sqrt{\mu_n \epsilon_n} = \frac{2\pi f}{c_0} \sqrt{\mu_n^r \epsilon_n^r}, \quad (21)$$

where  $\lambda_n, \mu_n$ , and  $\epsilon_n$  are the wavelength, permeability and permittivity of medium  $n$ , respectively,  $\omega$  stands for the angular frequency  $f$  refers to the frequency, and  $c_0$  is the speed of light in vacuum. In the rest of the paper, we consider  $\mu_n^r = 1$  for both media ( $n = 1$  is usually air, and  $n = 2$  is a non-magnetic dielectric material).

By inserting (19) and (20) in (17) and solving for the boundary condition at  $z = h$ , which is given by,

$$H_{\alpha'} \Big|_{z=h+} - H_{\alpha'} \Big|_{z=h-} = \sigma_{\alpha\alpha} E_{\alpha}, \quad (22)$$

the following dispersion equation for TM SPP waves in graphene is found [6], [14], [17]:

$$\frac{\epsilon_1^r}{\sqrt{k_{spp}^2 - \frac{\epsilon_1^r \omega^2}{c_0^2}}} + \frac{\epsilon_2^r}{\sqrt{k_{spp}^2 - \frac{\epsilon_2^r \omega^2}{c_0^2}}} = -i \frac{\sigma_{\alpha\alpha}}{\omega \epsilon_0}, \quad (23)$$

where all the parameters have already been defined. A closed-form solution for  $k_{spp}$  can only be obtained when considering a single isolated AGNR surrounded by air ( $\epsilon_1^r = \epsilon_2^r = 1$ ), which is not our case. For this, we numerically study the propagation index of TM SPP waves in the next section.

2) **TE Modes:** The propagation index for TE modes can be obtained by following a similar procedure to that for the TM case. In particular, first, by assuming that the magnetic field  $\vec{H}$  and electric field  $\vec{E}$  have a similar form to that of the electric field  $\vec{E}$  in (19) and the magnetic field  $\vec{H}$  in (20), second, by plugging this into the Maxwell's equations (17), and, third, by forcing the boundary condition at  $z = h$ , the following dispersion equation for the SPP wave vector  $k_{spp}$  can be found [14],

$$\sqrt{k_{spp}^2 - \frac{\omega^2}{c_0^2} \epsilon_1} + \sqrt{k_{spp}^2 - \frac{\omega^2}{c_0^2} \epsilon_2} + i\omega\mu_0\sigma_{\alpha'\alpha'} = 0, \quad (24)$$

where  $\omega$  is the angular frequency,  $\epsilon_n = \epsilon_0 \epsilon_n^r$  stands for the permeability of medium  $n$ ,  $c_0$  is the speed of light in vacuum,

$\mu_0$  is the permittivity of the medium  $n$ , and  $\sigma_{\alpha'\alpha'}$  is the AGNR conductivity for  $\alpha'$ -polarized waves given by (8). Moreover, a closed-form expression for  $k_{spp}$  can be found in this case,

$$k_{spp} = \frac{\omega}{c_0} \sqrt{\epsilon_1^r - \left( \frac{(\epsilon_1^r - \epsilon_2^r) + \sigma_{\alpha'\alpha'}^2 \eta_0^2}{2\sigma_{\alpha'\alpha'} \eta_0} \right)^2}, \quad (25)$$

where  $\eta_0 = \mu_0/\epsilon_0$ . Next, we numerically investigate the propagation of SPP TE modes in AGNRs.

## B. Numerical Analysis

In this section, we numerically study the propagation of SPP waves in semi-finite size graphene nanoribbons. As in Section III-C, we consider AGNRs with different widths, i.e.,  $W = 2.1$  nm ( $N = 18$ ),  $W = 10.1$  nm ( $N = 84$ ), and  $W = 50.0$  nm ( $N = 408$ ), as well as different chemical potential ( $\mu = 0$  eV and  $\mu = 0.3$  eV), at a temperature  $T = 300$  K. We consider the medium above the AGNR to be air ( $\epsilon_1^r = 1$ ) and the medium below the AGNR to be silicon dioxide  $\text{SiO}_2$  ( $\epsilon_2^r = 4$  for the frequency range considered in our analysis).

1) **TM Modes:** The propagation of TM SPP modes in graphene is governed by the dispersion equation given in (23). For a TM mode to exist, the real part of the SPP wave vector,  $\text{Re}\{k_{spp}\}$ , must be positive. As a result, from (23), TM modes along the  $\alpha$ -axis only exist if the imaginary part of the conductivity,  $\sigma_{\alpha\alpha}$ , is positive. This is in accordance with the results obtained for infinitely large graphene sheets in [14], [17], [20], [37]. As a result, based on the conductivity analysis in Section III-C, SPP TM modes only propagate in AGNRs with a chemical potential  $\mu > 0$ . In addition, TM modes are mainly supported along the  $x$ -axis or weakly along the  $y$ -axis in relatively wide ribbons (e.g.,  $W = 50.0$  nm).

In Fig. 4(a), we plot the real part of the SPP wave vector,  $\text{Re}\{k_{spp}\}$ , of TM modes propagating along the  $x$ -axis for a  $W = 2.1$  nm wide AGNR, with chemical potential  $\mu = 0.3$  eV, as a function of the frequency. The values are normalized by the wave vector in the medium 1,  $k_1$ . In the same figure, we illustrate the imaginary part of the conductivity for  $x$ -polarized radiation,  $\text{Im}\{\sigma_{xx}\}$  from (8), as a function of the frequency. The SPP wave vector is only defined at those frequencies for which the imaginary part of the complex conductivity for  $x$ -polarized radiation is positive. This is achieved when the conductivity is governed by intraband transitions (see Section III-C). We can see that the real

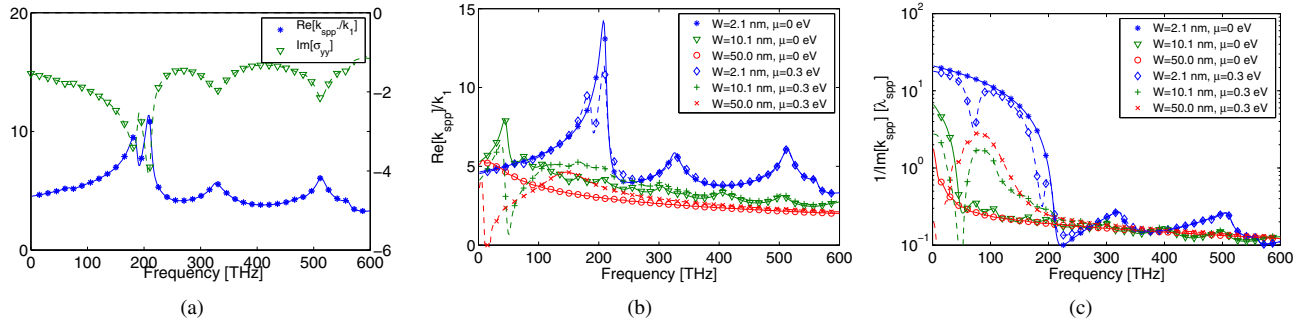


Fig. 5. (a) Real part of  $k_{spp}/k_1$  and imaginary part of  $\sigma_{yy}$  for an AGNR with  $W = 2.1$  nm, (b) Real part of  $k_{spp}/k_1$  for different AGNR width  $W$  and chemical potential  $\mu$ , and (c)  $1/e$ -amplitude decay propagation distance in terms of  $\lambda_{spp}$  for different AGNR width  $W$  and chemical potential  $\mu$  ( $T = 300$  K).

part of  $k_{spp}$  can be more than two orders of magnitude higher than that of the wave vector in medium 1, i.e., in the air.

In Fig. 4(b), the impact of the AGNR width on the propagation of TM SPP modes is illustrated, by plotting the real part of the SPP wave vector,  $\text{Re}\{k_{spp}\}$ , as a function of the frequency for different values of  $W$ . For  $W = 2.1$  nm, SPP modes appear mainly due to the forward intra-band transitions at frequencies close to 0 (the so-called Drude component) as well as right after the frequencies corresponding to inter-band transitions, due to backward intra-band transitions [29]. When the AGNR width increases, the conductivity is dominated by the forward intra-band transitions at frequencies close to 0. For relative wide AGNRs,  $W = 50.0$  nm, the conductivity tends to that of infinitely large graphene sheets, and the SPP wave vector tends to that of graphene [20]. The SPP mode compression factor,  $\text{Re}\{k_{spp}\}/k_1$  is lower for wider AGNRs. However, this higher compression comes at the cost of lower SPP propagation distances, as we discuss next.

In Fig. 4(c), we analyze the impact of the AGNR width on the propagation length of TM SPP modes in graphene, by plotting the inverse of the imaginary part of the SPP wave vector,  $1/\text{Im}\{k_{spp}\}$ , as a function of the frequency for different values of  $W$ . To better illustrate the propagation length of SPP waves, this is represented in terms of the SPP mode wavelength,  $\lambda_{spp}$  in (16). For example, the  $1/e$ -amplitude decay distance of TM SPP waves is on the order of a few SPP wavelengths for frequencies below 100 THz. We can see also that the width does not drastically impact the relative attenuation of the SPP waves on graphene, while, as we discussed above, narrower AGNRs allow more highly compressed SPP modes. Therefore, for thin AGNRs,  $\lambda_{spp} \ll \lambda_1$  specially for narrower AGNRs, while the relative SPP propagation length remains similar.

**2) TE Modes:** The propagation of TE SPP modes in graphene is governed by the dispersion equation given in (24). For a TE mode to exist, the real part of the SPP wave vector,  $\text{Re}\{k_{spp}\}$ , must be positive. As a result, from (24), TE modes along the  $x$ -axis only exist if the imaginary part of the conductivity,  $\sigma_{\alpha'\alpha'}$ , is negative. This is in accordance with the results obtained for infinitely large graphene sheets in [14], [26], [37]. As a result, based on the conductivity analysis in Section III-C, SPP TE modes can propagate in AGNRs with a chemical potential  $\mu \geq 0$ .

The real part of the SPP wave vector for TE modes propagating along the  $x$ -axis, normalized by the wave vector

in the medium 1,  $\text{Re}\{k_{spp}\}/k_1$ , is shown in Fig. 5(a), as a function of the frequency for a  $W = 2.1$  nm wide AGNR, with chemical potential  $\mu = 0.3$  eV. In the same figure, we illustrate the imaginary part of the conductivity for  $y$ -polarized radiation,  $\text{Im}\{\sigma_{yy}\}$  from (8). For this width  $W$  and chemical potential  $\mu$ , the SPP wave vector is for all the frequencies in our analysis, given that the imaginary part of the complex conductivity for  $y$ -polarized radiation is always negative. We can see that the real part of  $k_{spp}$  can be more than two orders of magnitude higher than that of the wave vector in medium  $n = 1$ , i.e., in the air.

In Fig. 5(b), the real part of the SPP wave vector for TE modes propagating along the  $x$ -axis, normalized by the wave vector in the medium 1,  $\text{Re}\{k_{spp}\}/k_1$ , is shown as a function of the frequency for different values of  $W$  and of the chemical potential  $\mu$ . TE SPP modes propagate along the  $x$ -axis mainly due to inter-band transitions. This can be clearly seen for example for  $W = 2.1$  nm, in which the SPP mode compression factor,  $\text{Re}\{k_{spp}\}/k_1$  can reach much higher values than for the rest of frequencies. When increasing the AGNR width, the major inter-band peaks are attenuated, and the same occurs with the SPP mode compression factor. As for the conductivity, the chemical potential does not drastically affect the propagation of TE SPP modes.

In Fig. 5(c), the inverse of the imaginary part of the SPP wave vector along the  $x$ -axis,  $1/\text{Im}\{k_{spp}\}$ , is shown as a function of the frequency for different values of  $W$  and  $\mu$ . This is plotted in terms of  $\lambda_{spp}$  in (16) to better understand its behavior. The  $1/e$ -amplitude decay distance of TE SPP waves is relatively larger in terms of  $\lambda_{spp}$ , but due to the much lower mode compression factor  $\text{Re}\{k_{spp}\}/k_1$ , the actual propagation length of TE SPP waves is similar or even slightly lower than that of TM modes. Finally, the propagation of TE SPP modes along the  $y$ -axis is also possible for those cases in which  $\text{Im}\{\sigma_{xx}\} < 0$ . However, these are only very weakly propagating modes.

## V. MODELING AND ANALYSIS OF GRAPHENE-BASED PLASMONIC NANO-ANTENNAS

In this section, we model and analyze our proposed graphene-based plasmonic nano-antenna. First, we highlight the differences between plasmonic antennas and classical metallic antennas. We then model the plasmonic nano-antenna as a resonant cavity and obtain its frequency response.

### A. Plasmonic Nano-antenna Theory

Plasmonic nano-antennas differ largely from classical metallic antennas. The main differences between plasmonic nano-antennas and metallic antennas are summarized as follows:

- **Finite Complex Conductivity:** In classical antenna theory, a common assumption is to model the material of the antenna building components as Perfect Electrical Conductor (PEC), i.e., as a material with infinite conductivity,  $\sigma_{PEC} \rightarrow \infty$ . This assumption simplifies the analytical study of the antenna by forcing the field inside the antenna  $\vec{E}^{in}$  to be zero. If the field were non-zero, the current inside the antenna would tend to infinite,  $\vec{J}^{in} \rightarrow \infty$ , as defined by the Ohm's law (18). Since infinite currents are not allowed,  $\vec{E}^{in}$  is required to be zero. On the contrary, a finite complex conductivity is required for the propagation of SPP waves, as given by (23) and (24). Moreover, this conductivity drastically changes with the size or chemical potential of the material.
- **Plasmonic Current Wave:** In classical antenna theory, the electrical current wave traveling along a PEC antenna propagates at the speed of light in vacuum  $c_0$  with wave vector  $k_0$ . On the contrary, the electrical current wave traveling along a plasmonic antenna propagates at the much lower SPP wave propagation speed with wave vector  $k_{spp}$ . Moreover, it is analytically proven in [5], that a plasmonic nano-antenna cannot support an additional current which propagates with  $k_0$ . This much slower propagation of the current wave is what allows the reduction of the physical antenna size in accordance with the SPP wave compression factor  $\text{Re}\{k_{spp}\}/k_1$ , given by (16). The wave vector of SPP waves depends strongly on the type of SPP modes and the size and chemical potential of the plasmonic nano-structure.

As a result of these two main differences, many other implications affect the design of plasmonic nano-antennas. For example, in classical antenna theory, when considering PEC materials, the resonant frequency of the fundamental dipole antenna depends only its length. However, for a plasmonic antenna, the resonant frequency of a nanowire-based dipole antenna, depends also on the temperature, chemical potential or radius of the wire, due to the impact of these parameters in its conductivity [5]. This can be extrapolated to other types of plasmonic nano-antennas [7], [21], [23].

### B. Frequency Response of Plasmonic Nano-antennas

We model our proposed graphene-based nano-antenna as a *plasmonic nanostrip antenna* [34], [39]. At the microscale, microstrip antennas (also known as planar antennas or printed antennas) have been widely used in many applications due to their simple manufacture, compatibility with planar circuitry, low profile, planar structure, and unidirectional radiation.

The two dimensional nature of graphene makes it, at least intuitively, a perfect candidate to port the advantages of microstrip antennas to the nanoscale. Contrary to carbon nanotube-based antennas [4], [13] or nano-wire-based antennas [5], the planar geometry of graphene is supposed to ease the integration of nano-antennas in advanced nano-devices

with diverse applications, such as, biological and chemical nanosensor networks [1] or optical interconnects in advanced multi-core computing architectures.

In order to analyze the frequency response of nano-strip antennas, we model the graphene-based heterostructure composed of the AGNR, the dielectric material and the ground plane, as a *plasmonic resonant cavity*. This imposes a condition of the AGNR length  $L$  for the antenna to resonate. Up to this point, in Section III and Section IV, we have analyzed the impact of the finite width  $W$  of the AGNR on its conductivity and on the propagation of SPP waves, while considering the length  $L$  of the AGNR to tend to infinite or, at least, to be much larger than  $W$ ,

$$L \gg W \gg h, \quad (26)$$

where  $h$  is the dielectric high. As discussed in Section III-C, and illustrated in Fig. 3, the conductivity of AGNRs tends to that of infinitely large graphene sheets as the width  $W$  increases. For example, for  $W = 50$  nm, the impact of the lateral confinement of electrons in the  $y$ -axis on the conductivity along the  $x$ -axis is almost negligible. Therefore, the length  $L$  of the AGNR does not impact the conductivity as long as we consider it to be in the order of a few hundreds nanometers. Similarly, as we discussed in Section IV-A, the dispersion of SPP modes in AGNRs given by (23) and (24) is determined by the permittivity of the surrounding media and the conductivity of the AGNR, but not by its length  $L$ . However, for the plasmonic nano-antenna to resonate, there is an additional constraint on the AGNR length, which depends on the type of SPP modes propagating along the antenna.

1) **TM Modes:** The condition on the nano-strip length  $L$  for a TM SPP wave mode to propagate along the  $x$ -axis is

$$L = m \frac{\lambda_{spp}}{2} = m \frac{\pi}{\text{Re}\{k_{spp}\}} \quad (27)$$

where  $m = 1, 2, \dots$ , and  $\lambda_{spp}$  and  $k_{spp}$  refer to the SPP wavelength and SPP wave vector, respectively. The SPP wave vector  $k_{spp}$  in (23) depends on the AGNR width  $W$  and chemical potential  $\mu$ . As a result, the resonant length  $L$  of the antenna, or inversely, the resonant frequency of a fixed length  $L$  AGNR depends also on these two parameters. Note the difference with classical metallic antennas, in which the wave vector in the vacuum  $k_0$  (or an equivalent effective wave vector  $k_{eff}$  which captures the impact of the dielectric and the ground plane) is used instead of the SPP wave vector  $k_{spp}$ .

In Fig. 6(a), we plot the resonant antenna length  $L$  (27) for the fundamental TM SPP mode ( $m = 1$ ) along the  $x$ -axis. As discussed in Section IV-A, SPP TM modes only exists at specific frequencies for which the imaginary part of the dynamic complex conductivity  $\sigma_{xx}$  is positive. For the frequencies that the TM mode exists, the wave compression factor  $\text{Re}\{k_{spp}\}/k_1$  allows for a much shorter  $L$  than that of classical metallic antennas. For example, an antenna with  $L = 1$   $\mu\text{m}$  and  $W = 2.1$  nm, at  $\mu = 0.3$  eV and  $T = 300$  K, approximately radiates at 8.5 THz (Fig. 6(b)). This is 35 times shorter than the size required for a metallic antenna operating at the same frequency. These results are consistent with our first hypothesis in [18], with the simulation-based analysis that we conducted in [22] for infinitely large graphene sheets, as

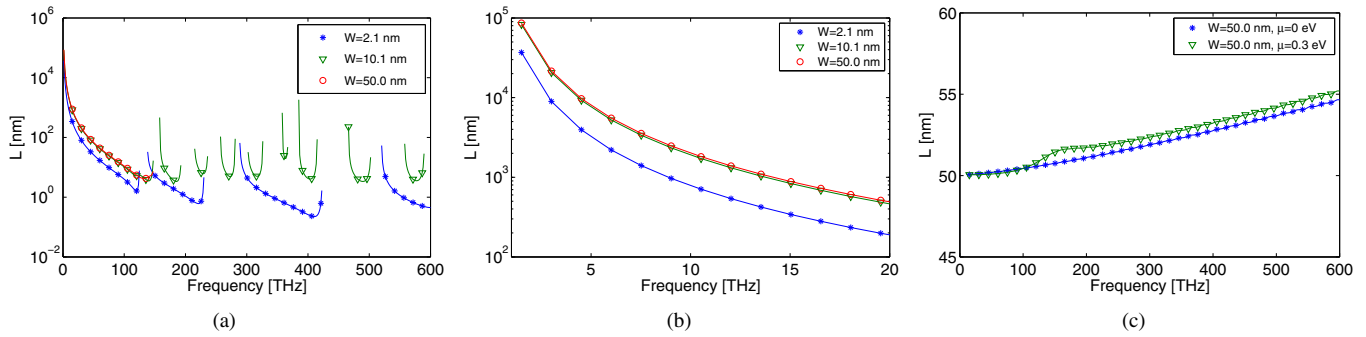


Fig. 6. (a) Antenna resonant length  $L$  for the fundamental TM mode ( $m = 1$  in (27)) ( $\mu = 0.3$  eV), (b) Antenna resonant length  $L$  for the fundamental TM mode in the Terahertz Band ( $\mu = 0.3$  eV), and (c) Antenna resonant length  $L$  for the fundamental TE mode ( $p = q = 1$  in (28)) ( $T = 300$  K).

well as, for the experimental SPP propagation measurements reported in [16], [19].

2) **TE Modes:** The condition on the nano-strip length  $L$  for a TE SPP wave mode to propagate along the  $x$ -axis is

$$L = \frac{2q - 1}{\sqrt{\left(\frac{2p-1}{W}\right)^2 - \left(\frac{2}{\lambda_{spp}}\right)^2}} = \frac{(2q - 1)\pi}{\sqrt{\left(\frac{(2p-1)\pi}{W}\right)^2 - \text{Re}\{k_{spp}\}^2}} \quad (28)$$

where  $p, q = 1, 2, \dots$ , and  $\lambda_{spp}$  and  $k_{spp}$  are the SPP wavelength and wave vector for TE SPP modes, respectively. The SPP wavevector  $k_{spp}$  given by (24) depends on the AGNR width  $W$  and chemical potential  $\mu$ . Therefore, there is a double dependance on the width  $W$  when determining the resonant length of TE modes in nano-strip antennas. In Fig. 6(c), the resonant antenna length  $L$  for TE modes is shown as a function of the frequency. However, as expected from 28, much higher frequencies are needed to actually see the impact of the length on the TE mode. Alternatively, much wider nano-strips can be considered, but in that case, rather than AGNRs, we would require the use of much larger graphene sheets.

Up to this point, we have discussed the frequency response of the antenna. However, little has been said about the efficiency of the antenna itself. Based on our numerical analysis in Section IV-B, the propagation length of the SPP modes in graphene given by  $1/\text{Im}\{k_{spp}\}$  is on the order of a few SPP wavelengths  $\lambda_{spp}$  which seems somehow desirable for the radiation from graphene-based heterostructures. However, the radiation principle itself might differ largely with the AGNR width. For example, for relatively wide nano-patches, it is common to model the antenna as four magnetic currents, one in each edge, two of them being radiative and two of them resulting in non-radiative. Our current and future work is aimed at characterizing the antenna efficiency and gain. While our study has been focused on AGNRs, a similar study can be conducted for ZGNRs, which would lead to similar results.

## VI. CONCLUSIONS

In this paper, we have proposed, modeled and analyzed a novel graphene-based plasmonic nano-antenna for communication among nano-devices. The proposed antenna is based on a thin graphene nanoribbon and reassembles a nano-strip antenna. We have first analytically and numerically computed the conductivity of semi-finite size graphene nanoribbons as a function of their width and chemical potential. Then, we have

extensively analyzed and discussed the propagation of SPP waves in GNRs for the first time. Finally, we have modeled our antenna as a plasmonic resonant cavity and obtained its frequency response. The results show that, by exploiting the high wave compression mode of SPP waves in AGNRs, graphene-based nano-antennas are able to work at much lower frequencies than classical metallic antennas of the same size. For example, a one-micrometer-long ten-nanometers-wide plasmonic nano-antenna is expected to radiate in the Terahertz Band (0.1-10 THz). This result has the potential to open the door to EM communication in nanonetworks.

## REFERENCES

- [1] I. F. Akyildiz and J. M. Jornet, "Electromagnetic wireless nanosensor networks," *Nano Commun. Netw. (Elsevier) J.*, vol. 1, no. 1, pp. 3–19, Mar. 2010.
- [2] T. Ando, Y. Zheng, and H. Suzuura, "Dynamical conductivity and zero-mode anomaly in honeycomb lattices," *J. Physical Soc. Japan*, vol. 71, no. 5, pp. 1318–1324, 2002.
- [3] J. E. Burke, "Analytical study of tunable bilayered-graphene dipole antenna," Army Armament Research, Development and Engineering Center, Dover, NJ, USA, Tech. Rep., Mar. 2011.
- [4] P. Burke, S. Li, and Z. Yu, "Quantitative theory of nanowire and nanotube antenna performance," *IEEE Trans. Nanotechnol.*, vol. 5, no. 4, pp. 314–334, July 2006.
- [5] J. Dorfmueller, R. Vogelgesang, W. Khunsin, C. Rockstuhl, C. Etrich, and K. Kern, "Plasmonic nanowire antennas: Experiment, simulation, and theory," *Nano Lett.*, vol. 10, no. 9, pp. 3596–3603, 2010.
- [6] A. A. Dubinov, V. Y. Aleshkin, V. Mitin, T. Otsuji, and V. Ryzhii, "Terahertz surface plasmons in optically pumped graphene structures," *J. Physics: Condensed Matter*, vol. 23, no. 14, p. 145302, 2011.
- [7] R. Esteban, T. V. Teperik, and J. J. Greffet, "Optical patch antennas for single photon emission using surface plasmon resonances," *Physical Rev. Lett.*, vol. 104, p. 026802, Jan. 2010.
- [8] L. Falkovsky and S. Pershoguba, "Optical far-infrared properties of a graphene monolayer and multilayer," *Physical Rev. B*, vol. 76, pp. 1–4, 2007.
- [9] L. Falkovsky and A. A. Varlamov, "Space-time dispersion of graphene conductivity," *European Physical J. B*, vol. 56, pp. 281–284, 2007.
- [10] A. K. Geim and K. S. Novoselov, "The rise of graphene," *Nature Materials*, vol. 6, no. 3, pp. 183–191, Mar. 2007.
- [11] V. P. Gusynin and S. G. Sharapov, "Transport of Dirac quasiparticles in graphene: Hall and optical conductivities," *Physical Rev. B*, vol. 73, p. 245411, June 2006.
- [12] V. P. Gusynin, S. G. Sharapov, and J. P. Carbotte, "AC conductivity of graphene: From tight-binding model to 2+1-dimensional quantum electrodynamics," *Int. J. Modern Physics B*, vol. 21, p. 4611, 2007.
- [13] G. W. Hanson, "Fundamental transmitting properties of carbon nanotube antennas," *IEEE Trans. Antennas Propag.*, vol. 53, no. 11, pp. 3426–3435, Nov. 2005.
- [14] —, "Dyadic Green's functions and guided surface waves for a surface conductivity model of graphene," *J. Applied Physics*, vol. 103, no. 6, p. 064302, 2008.

- [15] F. Hipolito, A. J. Chaves, R. M. Ribeiro, M. I. Vasilevskiy, V. M. Pereira, and N. M. R. Peres, "Enhanced optical dichroism of graphene nanoribbons," *Physical Rev. B*, vol. 86, p. 115430, Sep. 2012.
- [16] J. Horng, C.-F. Chen, B. Geng, C. Girit, Y. Zhang, Z. Hao, H. A. Bechtel, M. Martin, A. Zettl, M. F. Crommie, Y. R. Shen, and F. Wang, "Drude conductivity of Dirac fermions in graphene," *Physical Rev. B*, vol. 83, p. 165113, Apr. 2011.
- [17] M. Jablan, H. Buljan, and M. Soljačić, "Plasmonics in graphene at infrared frequencies," *Physical Rev. B*, vol. 80, p. 245435, Dec. 2009.
- [18] J. M. Jornet and I. F. Akyildiz, "Graphene-based nano-antennas for electromagnetic nanocommunications in the terahertz band," in *Proc. 4th European Conf. Antennas Propag. (EUCAP)*, Apr. 2010.
- [19] L. Ju, B. Geng, J. Horng, C. Girit, M. Martin, Z. Hao, H. Bechtel, X. Liang, A. Zettl, Y. R. Shen, and F. Wang, "Graphene plasmonics for tunable terahertz metamaterials," *Nature Nanotechnol.*, vol. 6, pp. 630–634, Sep. 2011.
- [20] F. H. L. Koppens, D. E. Chang, and F. J. Garcia de Abajo, "Graphene plasmonics: A platform for strong light matter interactions," *Nano Lett.*, vol. 11, no. 8, pp. 3370–3377, Aug. 2011.
- [21] J. Lim, C. Kim, J. jang, H. Lee, Y. jung, J. Kim, S. Park, B. Lee, and M. Lee, "Design of a subwavelength patch antenna using metamaterials," in *Proc. 38th European Microwave Conf. (EuMC)*, Oct. 2008, pp. 1246–1249.
- [22] I. Llatser, C. Kremers, A. Cabellos-Aparicio, J. M. Jornet, E. Alarcon, and D. N. Chigrin, "Graphene-based nano-patch antenna for terahertz radiation," *Photonics Nanostructures - Fundamentals Appl.*, vol. 10, no. 4, pp. 353–358, Oct. 2012.
- [23] C. Manolatu and F. Rana, "Subwavelength nanopatch cavities for semiconductor plasmon lasers," *IEEE J. Quantum Electron.*, vol. 44, no. 5, pp. 435–447, May 2008.
- [24] S. A. Mikhailov, "Theory of the giant plasmon-enhanced second-harmonic generation in graphene and semiconductor two-dimensional electron systems," *Physical Rev. B*, vol. 84, p. 045432, July 2011.
- [25] P. Mukherjee and B. Gupta, "Terahertz (THz) frequency sources and antennas - A brief review," *Int. J. Infrared Millimeter Waves*, vol. 29, no. 12, pp. 1091–1102, Dec. 2008.
- [26] A. Y. Nikitin, F. Guinea, F. J. Garcia-Vidal, and L. Martin Moreno, "Edge and waveguide terahertz surface plasmon modes in graphene microribbons," *Physical Rev. B*, vol. 84, p. 161407, Oct. 2011.
- [27] K. S. Novoselov, A. K. Geim, S. V. Morozov, D. Jiang, Y. Zhang, S. V. Dubonos, I. V. Grigorieva, and A. A. Firsov, "Electric field effect in atomically thin carbon films," *Science*, vol. 306, no. 5696, pp. 666–669, 2004.
- [28] N. Peres, A. Castro Neto, and F. Guinea, "Conductance quantization in mesoscopic graphene," *Physical Rev. B*, vol. 73, no. 19, p. 195411, May 2006.
- [29] K.-I. Sasaki, K. Kato, Y. Tokura, K. Oguri, and T. Sogawa, "Theory of optical transitions in graphene nanoribbons," *Physical Rev. B*, vol. 84, p. 085458, Aug. 2011.
- [30] K.-I. Sasaki, K. Kato, Y. Tokura, S. Suzuki, and T. Sogawa, "Pseudospin for Raman  $d$  band in armchair graphene nanoribbons," *Physical Rev. B*, vol. 85, p. 075437, Feb. 2012.
- [31] K.-I. Sasaki, K. Wakabayashi, and T. Enoki, "Electron wave function in armchair graphene nanoribbons," *J. Physical Soc. Japan*, vol. 80, no. 4, p. 044710, 2011.
- [32] G. Slepyan, M. Shuba, A. Nemilentsau, and S. Maksimenko, "Electromagnetic theory of nanodimensional antennas for terahertz, infrared and optical regimes," in *Proc. 12th Int. Conf. Mathematical Methods Electromagnetic Theory (MMET)*, July 2008, pp. 118–123.
- [33] S. Smaili, V. Singal, and Y. Massoud, "On the effect of width of metallic armchair graphene nanoribbons in plasmonic waveguide applications," in *Proc. 7th IEEE Int. Conf. Nano/Micro Engineered Molecular Syst. (NEMS)*, Mar. 2012, pp. 623–626.
- [34] T. Sondergaard, J. Beermann, A. Boltasseva, and S. I. Bozhevolnyi, "Slow-plasmon resonant-nanostrip antennas: Analysis and demonstration," *Physical Rev. B*, vol. 77, p. 115420, Mar. 2008.
- [35] T. Stauber, N. M. R. Peres, and A. K. Geim, "Optical conductivity of graphene in the visible region of the spectrum," *Physical Rev. B*, vol. 78, p. 085432, Aug. 2008.
- [36] P. Tassin, T. Koschny, M. Kafesaki, and C. M. Soukoulis, "A comparison of graphene, superconductors and metals as conductors for metamaterials and plasmonics," *Nature Photonics*, vol. 6, no. 4, pp. 259–264, Mar. 2012.
- [37] A. Vakil and N. Engheta, "Transformation optics using graphene," *Science*, vol. 332, no. 6035, pp. 1291–1294, June 2011.
- [38] K. Wakabayashi, K. Sasaki, T. Nakanishi, and T. Enoki, "Electronic states of graphene nanoribbons and analytical solutions," *Science Technol. Advanced Materials*, vol. 11, no. 5, p. 054504, 2010.
- [39] I. Wang and Y. Ping Du, "Optical input impedance of nanostrip antennas," *Optical Eng.*, vol. 51, no. 5, p. 054002, 2012.
- [40] Z. L. Wang, "Towards self-powered nanosystems: From nanogenerators to nanopiezotronics," *Advanced Functional Materials*, vol. 18, no. 22, pp. 3553–3567, 2008.
- [41] P. West, S. Ishii, G. Naik, N. Emani, V. Shalaev, and A. Boltasseva, "Searching for better plasmonic materials," *Laser Photonics Rev.*, vol. 4, no. 6, pp. 795–808, 2010.



**Josep Miquel Jornet** received the engineering degree in telecommunications engineering and the master of science in information and communication technologies from the Universitat Politècnica de Catalunya, Barcelona, Spain, in 2008. He received the Ph.D. degree in electrical and computer engineering from the Georgia Institute of Technology, Atlanta, GA, in 2013. He is currently an Assistant Professor with the Department of Electrical Engineering at the University at Buffalo, The State University of New York. From September 2007 to

December 2008, he was a visiting researcher at the Massachusetts Institute of Technology, Cambridge, under the MIT Sea Grant program. He was the recipient of the Oscar P. Cleaver Award for outstanding graduate students in the School of Electrical and Computer Engineering at the Georgia Institute of Technology in 2009. He also received the Broadband Wireless Networking Lab Researcher of the Year Award at the Georgia Institute of Technology in 2010. He is a member of the IEEE and the ACM. His current research interests include electromagnetic nanonetworks, graphene-enabled wireless communication, terahertz band communication networks, and the Internet of Nano-Things.



**Ian F. Akyildiz** received the B.S., M.S., and Ph.D. degrees in computer engineering from the University of Erlangen-Nürnberg, Germany, in 1978, 1981, and 1984, respectively. Currently, he is the Ken Byers Chair Professor in Telecommunications with the School of Electrical and Computer Engineering, Georgia Institute of Technology, Atlanta, the Director of the Broadband Wireless Networking (BWN) Laboratory, and the Chair of the Telecommunication Group at Georgia Tech. Since 2013, he has been a FiDiPro Professor (Finland Distinguished Professor

Program (FiDiPro) supported by the Academy of Finland) in the Department of Electronics and Communications Engineering at Tampere University of Technology, Finland, and the founding director of NCC (Nano Communications Center). Since 2008, he has also been an honorary professor with the School of Electrical Engineering at Universitat Politècnica de Catalunya (UPC) in Barcelona, Catalunya, Spain and the founding director of N3Cat (NaNoNetworking Center in Catalunya). He is the Editor-in-Chief of *Computer Networks Journal* (Elsevier), founding Editor-in-Chief of the *Ad Hoc Networks Journal* (Elsevier), the *Physical Communication Journal* (Elsevier) and the *Nano Communication Networks Journal* (Elsevier). He is an IEEE Fellow (1996) and an ACM Fellow (1997). He received numerous awards from IEEE and ACM. His current research interests are in nanonetworks, long term evolution advanced (LTE-A) networks, cognitive radio networks, and wireless sensor networks.